THE JOURNAL OF PHYSICAL CHEMISTRY B

Article

Cite This: J. Phys. Chem. B 2019, 123, 8247−8260

pubs.acs.org/JPCB

Experimental and Molecular Dynamics Simulation Study of the Effects of Lignin Dimers on the Gel-to-Fluid Phase Transition in DPPC Bilayers

Xinjie Tong,[†] Mahsa Moradipour,[‡] Brian Novak,[†] Poorya Kamali,[§] Shardrack O. Asare,[§] Barbara L. Knutson,[‡] Stephen E. Rankin,[‡] Bert C. Lynn,[§] and Dorel Moldovan*[,†,∥]

[†]Department of Mechanical and Industrial Engineering, Louisiana State University, Baton Rouge, Louisiana 70803, United States

[‡]Department of Chemical and Materials Engineering, University of Kentucky, Lexington, Kentucky 40506, United States

[§]Department of Chemistry, University of Kentucky, Lexington, Kentucky 40506, United States

[∥]Center for Computation and Technology, Louisiana State University, Baton Rouge, Louisiana 70803, United States

Supporting Information

ABSTRACT: High resolution differential scanning calorimetry (DSC) and molecular dynamics (MD) simulations were used to investigate the effect of three lignin dimers on the gel to fluid phase transition in DPPC lipid bilayers. The goal of this research is to begin to understand the partitioning of model lignin dimers into lipid bilayers and its effects on the gel to fluid transition temperature (T_m). The long-term objective is to establish structure−function relationships for well-defined lignin derivatives at biologically relevant surfaces. This work uses a newly synthesized guiacylglycerol guaiacol ester with a hydroxypropenyl (HOC_3H_4-) group resembling natural lignin (GG dimer), compared with a truncated GG dimer without the HOC_3H_4- and benzyl-modified GG dimers. The DSC results show that the dimer most like natural lignin (with a hydroxypropenyl tail) has log $K = 2.72 \pm 0.05$, and MD simulations show that it associates with the headgroups of the lipid but does not penetrate strongly into the interior of the bilayer. Therefore, this dimer has little effect on the T_m value. In contrast, the truncated dimer, which has been used as a representative GG dimer in prior studies, partitions into the bilayer, as seen in MD simulations, and shifts T_m because of its increased lipophilicity (DSC log $K = 3.45 \pm 0.20$). Similarly, modification of the natural GG dimer by benzylation of the phenol makes it lipophilic (DSC log $K = 3.38 \pm 0.28$), causing it to partition into the bilayer, as seen in MD simulations and shift T_m. In MD, we capture the transition from gel to fluid phase by defining and analyzing a normalized deuterium order parameter averaged over all carbon atoms located in the middle of the lipid tails. In this way, the phase transition can be clearly observed and, importantly, MD results show the same trend of transition temperature shifts as the DSC results. Furthermore, we compare partition coefficients estimated from free energy profiles calculated in MD to those obtained from experiment and they are in qualitative agreement. The success at predicting the structural effects of lignin dimers on lipid bilayers suggests that MD simulations can be used in the future to screen the interactions of lignin oligomers and their derivatives with lipid bilayers.

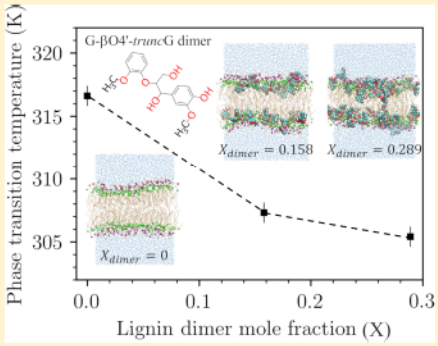

INTRODUCTION

Lignin is one of the most abundant biopolymers in nature and is found mostly in cell walls of plants. It is a polymer composed of the aromatic monomers (so-called monolignols) *p*-coumaryl alcohol, coniferyl alcohol, and sinapyl alcohol that bind to each other via radical coupling and form a complex, heterogeneous structure. In plants, lignin plays important roles in structuring cell walls and preventing water penetration through the xylem. It has also been documented to have important roles in plant and tree defense against microbial attack.[1] Because it is naturally biodegradable, biocompatible, and has good stability and low toxicity, lignin derivatives are under investigation for multiple pharmacological and biomedical applications.[2] It has also been proven that lignin and its derivatives (a.k.a. "lignins") have antioxidant and antibacterial properties and they have already been used for the treatment of various diseases including diabetes, HIV, and cancer.[2,3] The use of lignin nanoparticles (LNPs) in drug delivery has been reported in many studies.[4,5] Besides benefits to human health, purified lignin and specific lignins have the potential to improve livestock intestine morphology and to control pathogens.[6] In many of these applications, the effects of lignins could be explained by the antioxidant capacity conferred by the phenolic character of its constituents.[7] It has been documented that low-molecular-weight oligomers derived from guaiacyl units are central to the antioxidant properties of lignins.[8] Often, in these

Received: June 10, 2019
Revised: September 5, 2019
Published: September 5, 2019

DOI: 10.1021/acs.jpcb.9b05525
J. Phys. Chem. B 2019, 123, 8247−8260

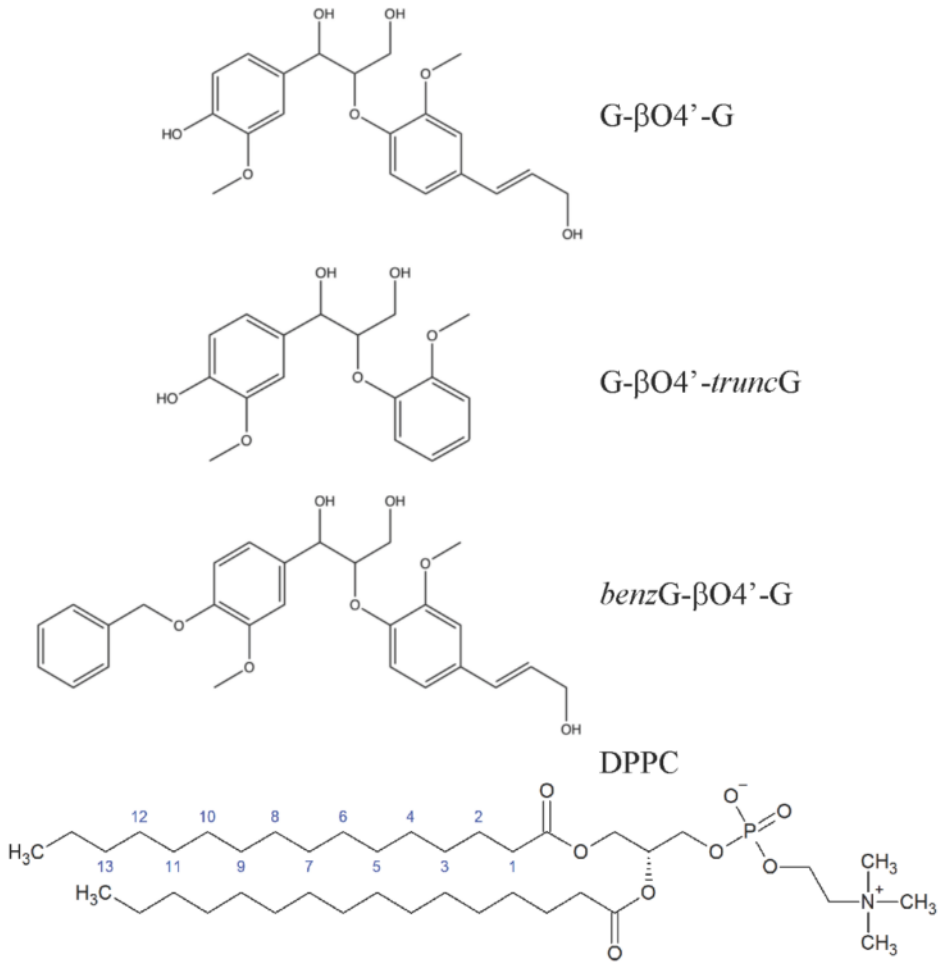

Figure 1. Structure of the molecules used in the experimental and simulation investigations.

applications, lignin absorbs into or binds to cell membranes or to membrane embedded molecular structures, such as proteins. For this reason, the investigation of the interaction of lignins with cell membranes is of critical importance.

Cell membranes are primarily comprised of lipids. In the physiological state, lipid bilayers are in their fluid state and this fluidity is pivotal to cell functions. The gel−fluid transition temperature (T_m) of lipid bilayers is the temperature where the lipids change from a gel phase where they are tightly packed in ordered domains to a more loosely packed fluid phase. Interactions between compounds such as drugs and lipid bilayers can affect their structure and permeability, and therefore T_m. Conversely, important changes in lipid and bilayer dynamics occur near the transition. For example, it was reported that the protein-mediated exchange of lipids between vesicles was greatly increased near the transition temperature.[9] Lipid transfer processes are essential to biological function.

Additive-induced changes in T_m depend on both the molecular structure and concentration of the additives as well as the identity of the lipids, since these factors determine the location and concentration of the additives in the bilayer. This is supported by multiple experimental investigations. Jain examined the effect of a variety of small molecules including alkanols, fatty acids, detergents, and ionophores on dipalmitoyl lecithin bilayer phase behavior.[10] The plant-derived flavonoids quercetin, hesperetin, and naringenin were reported to lower the T_m of 1,2-dipalmitoyl-*sn*-glycero-3-phosphocholine (DPPC) liposomes, while rutin (also a flavonoid) did not.[11] Prenyl-modified isoflavones had a more noticeable effect on the T_m of DPPC than nonprenylated ones.[12] T_m was reduced by more than 10 K with broader transition peaks when adding a high concentration (20%) of isoflavone. Ojogun et al. investigated the partitioning and phase behavior of a series of nicotinic acid esters (nicotinates) between aqueous solution and DPPC membrane bilayers.[13] High concentrations of nicotinates increased the main phase transition temperature and decreased the membrane partition coefficient. Zhao et al. investigated the effects of cholesterol and paclitaxel on the phase behavior of DPPC liposomes, finding that both fluidize the bilayer.[14] Given that some lignin derivatives have polyphenolic drug-like structures, it is of interest to investigate their partitioning into lipid bilayers through effects on T_m.

Molecular dynamics (MD) simulation is a useful tool to gain information at the microscopic level and has contributed to understanding lipid bilayer phase behavior. However, most previous studies consider either pure lipids or lipid mixtures without additives[15−18] and most with additives were performed with coarse-grained models.[19−22] Atomistic studies of lipid bilayer phase transitions with additive molecules are still rare because of the time and length scale limitations of MD.

There are two approaches to estimate transition temperature using MD. The first approach is to mimic what is done experimentally by either heating a gel phase or performing several simulations at different temperatures starting from gel

DOI: 10.1021/acs.jpcb.9b05525
J. Phys. Chem. B 2019, 123, 8247−8260

phase configurations. Leekumjorn and Sum[15] did heating and cooling scans for DPPC and 1,2-dipalmitoyl-*sn*-glycero-3-phosphoethanolamine (DPPE) from 250 to 350 K and back to 250 K where the temperatures are in the range of the gel−fluid transitions. Simulations using the Berger parameters for DPPC showed clear changes in the slope of the enthalpy during heating simulations, allowing for easy identification of the phase transition.[16] Qin and Yu studied 1,2-disteroyl-*sn*-glycero-3-phosphocholine (DSPC) and 1,2-disteroyl-*sn*-glycero-3-phosphoethanolamine (DSPE) and found three stages during the DSPC transition which were from cross-tilted packing to tilted packing, tilted to "mixed" alignment, and "mixed" alignment to disordered, while DSPE did not have the "mixed" alignment state.[17] The second MD method involves simulating the gel and fluid phases in coexistence at various temperatures to find the temperature where neither phase grows. Coppock and Kindt used this method with DPPC and DSPC.[18]

There is little existing work related to the interaction of lignin dimers and derivatives with lipid bilayers, and we are not aware of any study of their effect on the gel−fluid transition temperature. The transport of lignin monomers across the plant cell membrane has been studied and seems to involve ATP-binding cassette transporters.[23−26] Boija and Johansson studied the partitioning of monolignol and dilignol model substances in liposomes using immobilized liposome chromatography and concluded that passive diffusion of some lignin precursors may be possible.[1] None of the compounds they considered are the same as those we consider here. Simulations of the interaction of lignin dimers with cellulose have been performed,[27] but we are not aware of any MD related to their interaction with lipid bilayers.

Here we studied the interaction of three derivatives of β-O-4′ linked dimers of coniferyl alcohol (GG) with DPPC bilayers with the aim of developing a molecular-level understanding of how these molecules affect the gel−fluid phase behavior of the bilayers. The derivatives considered are shown in Figure 1 and are the unmodified dimer, a truncated analogue, and a benzyl modified dimer. We investigated the interaction of these molecules with liposomes of DPPC using high resolution differential scanning calorimetry (DSC) and MD simulations. The DSC instrument incrementally changes the temperature of a sample and measures the heat flow. DSC allows phase transition temperatures to be identified easily by a peak in the heat flow, and we applied it to identify the transition temperature of liposomes between gel and fluid phases.[28] Gel−fluid transition temperatures calculated from MD simulations showed the same trend as DSC results, and the simulations also helped to explain how the lipids were affected by the lignin dimers.

■ MATERIALS AND METHODS

Experimental Details. Isopropanol (99%), hydrochloric acid (36.5−38%), 200 proof ethanol, acetone (99.5%), methylene chloride, anhydrous tetrahydrofuran, chloroform (99.8%), and deionized water (ASTM type II) were purchased from VWR International. Vanillin (99%), anhydrous potassium carbonate, (99%), tetrabutylammonium fluoride, diisobutyl aluminum hydride, sodium bis(trimethylsilyl) amide (95%), and ethyl bromoacetate (98%) were purchased from Alfa Aesar. *N*,*N*-Dimethylhexadecylamine (DMHA, ≥98%) and guaiacylglycerol-beta-guaiacyl ether (≥97%) were purchased from TCI America. Imidazole (99%) was purchased from Fisher Scientific. Phosphate buffered saline (PBS) was purchased from Sigma-Aldrich. 1,2-Dipalmitoyl-*sn*-glycero-3-phosphocholine (DPPC) was purchased from Avanti Polar Lipids (Alabaster, USA).

Lignin Dimer Synthesis. The structures of the three lignin dimers used in the study are summarized in Figure 1. The synthesis of 1-(4-hydroxy-3-methoxyphenyl)-2-[2-methoxy-4-(3-hydroxyprop-1-en-1-yl)phenoxy]propane-1,3-diol, which is abbreviated as G-βO4′-G, was done as described by Asare et al.[29] This dimer has the same β-O-4′ linked units in the core as the commercially available G-βO4′-*trunc*G dimer (guaiacylglycerol-β-guaiacyl ether) but with a 3-hydroxyprop-1-enyl tail. The synthesis of benzyl-modified GG dimer 1-(4-benzyloxy-3-methoxyphenyl)-2-[2-methoxy-4-(3-hydroxyprop-1-en-1-yl)-phenoxy]propane-1,3-diol (*benz*G-βO4′-G) proceeded with a small modification of the G-βO4′-G synthesis method such that the phenol group in the A ring of vanillin was protected with a benzyl group instead of the triisopropylsilyl group that was used for G-βO4′-G. To do this, a 0.5 M solution of vanillin in acetone was added to benzyl bromide in the presence of potassium carbonate. A molar ratio of 1 vanillin:1.5 benzyl bromide:1.5 potassium carbonate was used. At the end of the β-O-4 coupling reaction, the deprotection step was omitted from the original (G-βO4′-G) protocol and the benzyl group remained at the phenol terminus of the dimer.

Differential Scanning Calorimetry. To perform DSC experiments, DPPC liposomes in solution were made with varying amounts of lignin GG dimers following the traditional thin-film method described elsewhere.[14,13] Initially, GG dimers were mixed with 10 mg of DPPC to obtain mixtures of DPPC/dimer with dimer mole fraction ranging from 0 up to 0.40. Then, each one of the mixtures was dissolved in 1 mL of chloroform separately. The chloroform was then evaporated using a nitrogen gas stream to form lipid films in the bottom of the vials. To ensure that the chloroform evaporated completely, the vials were placed inside a vacuum chamber overnight. In the next step, lipids were rehydrated by addition of 1 mL of PBS buffer, making them rearrange into bilayers. Next, the bilayers were agitated and detached from the vial surfaces to form liposomes. Finally, the liposomes were extruded sequentially through a 200 nm polycarbonate membrane at a temperature above the gel−fluid transition temperature of the lipid (T_m = 315.3 ± 0.15 K) to make unilamellar liposomes of uniform size. Extrusion using membranes with 200 nm pore size yields homogeneous liposomes with an average diameter of ∼260 nm in the final suspension.[30,31] This protocol was conducted for making DPPC/G-βO4′-*trunc*G, DPPC/G-βO4′-G, and DPPC/*benz*G-βO4′-G mixtures in all of which various amounts of the lignin dimers were added to 10 mg of DPPC in 1 mL of PBS. Portions of 500 μL of the DPPC/dimer solutions were weighed into 1 mL ampules of a multicell differential scanning microcalorimeter (MC-DSC, TA Instruments, New Castle, DE), and the ampules were placed inside the machine. Samples were first heated to 328 K, then cooled to 283 K, and finally reheated from 283 to 328 K at 1 K/min. The main phase transition temperature of the samples was determined using *Nano-Analyzer* software.

Partition Coefficient from DSC. The partition coefficient of the dimers between the DPPC liposomes and aqueous solution (K) is related to the shift in transition temperature relative to pure DPPC liposomes. In the low concentration

DOI: 10.1021/acs.jpcb.9b05525
J. Phys. Chem. B 2019, 123, 8247−8260

limit, K was estimated using the relation proposed by Inoue et al.[32]

$$-\Delta T_m = \left\{ \frac{R \times {T_m}^2}{\Delta H_{DPPC}} \times \frac{K}{55.5 + C_{DPPC} \times K} \right\} C_s \quad (1)$$

This equation assumes that at equilibrium the depression in the main phase transition temperature is directly proportional to the amount of the dimer that partitions into the lipid bilayer.[13] In this equation, ΔT_m is the difference between the transition temperature of the sample and pure DPPC liposomes, T_m is the transition temperature of pure liposomes, R is the ideal gas constant, ΔH_{DPPC} is the phase transition enthalpy (31.4 kJ/mol), C_{DPPC} is the concentration of DPPC in PBS (0.0136 M), and C_s is the concentration of the dimers in PBS (M).[32] Solvent (PBS) is assumed to have the molar concentration of water (55.5 M). To solve for the partition coefficient, the entire constant in brackets was found using linear regression in the limit of low C_s. The partition coefficient values are reported as log(K).

Simulation Details. The MD simulation systems contained 128, 256, or 512 DPPC lipid molecules organized into flat bilayers, water, and one of the three variants of G−G lignin dimers. The bilayers were well hydrated with about 50 water molecules per lipid. All simulations were performed with the GROMACS 2016.3 package.[33] Constant number of atoms, pressure, and temperature (NPT) conditions were used for all simulations with a time step of 3 fs and fully periodic boundary conditions. The Berendsen barostat was used with a reference pressure of 1.0 bar and a time constant of 2.5 ps. The v-rescale thermostat[34] was used with a time constant of 0.1 ps. The cutoff for van der Waals interactions and short-range Coulomb interactions was 1.4 nm. The particle mesh Ewald (PME) method was used for long-range Coulomb interactions.

The interactions between atoms were described by the GROMOS 54a7 united atom force field[35] with the SPC water model.[36] Force field parameters exist for DPPC lipids, and the topology file can be downloaded from the Automated Topology Builder (ATB) Web site.[37] To obtain parameters for the lignin molecules, several small molecules representing fragments of the lignin molecules were submitted to ATB. ATB output force constants for a few bonded interactions (bond angles in particular) which were clearly several times larger than typical values, and they were modified to more reasonable values obtained from other molecules on ATB with structures containing that type of interaction. To validate whether parameters obtained using ATB are reasonably accurate, a simulation of solid erythro-2-(2,6-dimethoxy-4-methylphenoxy)-1-(4-hydroxy-3,5-dimethoxyphenyl)-propane-1,3-diol (EPD) was run, as reported by Langer et al.[38] EPD has a structure which is a very similar to a lignin dimer. Average unit cell dimensions and two average dihedral angles were compared with the results from experimental data. Details on the construction and validation of the lignol parameters are included in the Supporting Information.

We started with a pre-equilibrated DPPC lipid bilayer with 128 lipids (64 for upper and lower leaflets) which was available for download from the Lipidbook Web site[39] which is a public repository of force-field parameters for lipid membrane simulations. PACKMOL[40] was used to add more water molecules. The system was initially equilibrated at 326 K and 1.0 bar using semiisotropic pressure coupling. For single dimer simulatons, the dimer was then added away from the bilayer in water and overlapping waters were removed. For G-βO4′-G and G-βO4′-*trunc*G dimers at high concentrations, six dimers were then added at a time to each side of the bilayer. For *benz*G-βO4′-G dimers at high concentrations, only one dimer was added at a time to each side of the bilayer to avoid aggregation before reaching the bilayer (see Figure 2). The

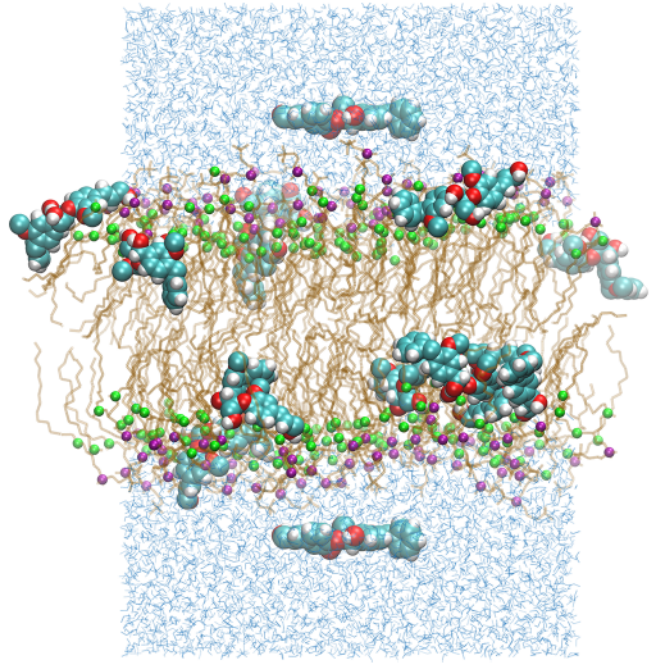

Figure 2. Snapshot depicting the preparation stage of a DPPC lipid bilayer, containing 0.289 mole fraction of *benz*G-βO4′-G dimers by gradually adding one dimer at a time on each side of the bilayer followed by a waiting period for dimers to adsorb into the bilayer prior to adding more dimers.

dimers were placed in water at around 1.25 nm away from the bilayer water interface defined by the averaged position of lipid phosphorus atoms, and as shown by the analysis of the simulations, it took about 1−2 ns until they were adsorbed onto the lipid bilayer surface. This time is long enough for dimers to undergo significant translational and rotational diffusion which ensured that the dimers lost memory of their initial orientations before adsorption to the bilayer. After a short simulation, the dimers adsorbed into the bilayer and then another 12 or 2 dimers were added, and the process was repeated until reaching the desired concentration. Lignin molecules were repelled when they came within 0.2 nm of box boundaries in the bilayer normal direction using a flat bottom potential with a force constant of 1000 kJ/(mol × nm^2) so that the number of lignin molecules entering each leaflet of the bilayer was equal. Systems which were 4 times larger (512 lipids) are also constructed by duplicating the smaller systems after adding lignin dimers.

Potential of Mean Force (PMF). The potential of mean force (PMF) can be used to approximate free energy differences as a function of one or more reaction coordinates, which in the case of lipid bilayers are often distances of molecules from the bilayer center. The PMF curve is related to the probabilities of observing different values of the reaction coordinate(s), and for lipid bilayers, it is useful for estimating the most probable location(s) of molecules relative to the lipid molecules using the Boltzmann distribution,

DOI: 10.1021/acs.jpcb.9b05525
J. Phys. Chem. B 2019, 123, 8247−8260

$$p(i) = \frac{e^{-\beta PMF(i)}}{\sum_{i=1}^{n} e^{-\beta PMF(i)}}$$

In the case where the desired range of reaction coordinate(s) can be adequately sampled in unbiased simulations, the PMF curve can be obtained directly from those probabilities. In most cases, in order to achieve adequate sampling over the whole range of reaction coordinate(s), the system must be biased. Umbrella sampling is an approach which involves biasing the system near different values of the reaction coordinate(s) in separate simulations (windows).

We computed PMFs in systems containing 128 DPPC molecules and a single lignin GG dimer. All three dimer variants were considered. Umbrella sampling[41] was used to calculate the PMF as a function of the distance from the center of mass of each lignin dimer to the center of the lipid bilayer along the bilayer normal direction. The window spacing was 0.1 nm, and 38 windows were used with equilibrium distances from 0.0 to 3.8 nm. Some starting configurations were simply extracted from initial unbiased simulations. Configurations for distances near the bilayer center that could not be obtained from the unbiased simulations were obtained by dragging the lignin molecule to the desired position at a rate of 0.00003 nm/ps. The umbrella potentials were harmonic restraints with force constants of 3000 kJ/(mol × nm^2). Umbrella sampling simulations were run at 326 K and 1.0 bar for 80 ns for each window where 30 ns was used for the equilibration time. The weighted histogram analysis method[42] is then applied to construct the unbiased PMF by combining data from all windows.

Partition Coefficient from MD. The partition coefficient K between two bulk phases is

$$K = e^{-\beta \Delta G} = e^{-\Delta G/RT} \tag{2}$$

where R is the gas constant, T is the temperature, and ΔG is the free energy difference between bulk phases. In MD simulations, the free energy difference can be obtained using the PMF as described above. However, an additional complication with lipids is that lipid bilayers are heterogeneous; there is no bulk lipid phase. This, in general, requires averaging the PMF[43] and perhaps defining a boundary between phases.

Various approximations can be made in defining the partition coefficient. When the difference between the minimum value of the PMF (PMF_{min}) and the value of PMF in bulk solution PMF_{sol} is large and the PMF curve is steep near its minimum, $\Delta G \approx PMF_{min} - PMF_{sol}$. The entire region of the system which affects the PMF of the molecule including the bilayer and interfacial water could be considered as one phase and bulk solution as the other phase. In that case, a Boltzmann weighted average of the PMF can be used

$$\log(K) = -\beta \Delta G_{avg} \approx -\beta \frac{\int_0^{z_{bulk}} PMF(z) e^{-\beta PMF(z)}\, dz}{\int_0^{z_{bulk}} e^{-\beta PMF(z)}\, dz} \tag{3}$$

where the PMF in bulk solution at a distance z_{bulk} from the bilayer center is set to 0. However, this definition is not appropriate for comparison to the partition coefficient, K, obtained from DSC based on eq 1, since the molecules outside the bilayer will not affect the transition temperature. We need to define a boundary between the lipid and solution phases. This is somewhat arbitrary, but we assume that the boundary is the average distance of the lipid phosphorus atoms from the bilayer center (z_{phos}), since anything outside the head groups of the lipids will have little effect on the transition temperature. We use the following definition of the partition coefficient.[44]

$$\log(K) \approx -\beta(PMF_{avg,l} - PMF_{avg,w}) + \log\left(\frac{V_w}{V_l}\right) \tag{4}$$

$PMF_{avg,l}$ and $PMF_{avg,w}$ are the Boltzmann weighted average values of the PMF in the lipid phase and solution phase, respectively. They were calculated as in eq 3 except the bounds on the integrals are from 0 to z_{phos} and from z_{phos} to the furthest distance in the PMF curve, respectively. V_w and V_l are the volumes of the water and lipid phases, respectively, and were defined by the same bounds as in the integrals.

Transition Temperature. One way to estimate a transition temperature is to simply simulate the two phases in coexistence in one simulation box. At the transition temperature, the system will remain in coexistence. At temperatures above or below the transition temperature, one phase will grow at the expense of the other and eventually only one phase will exist. This method has been used for lipids[18] and was termed the stripe growth method.

We used the coexistence method with a DPPC bilayer. First, a gel phase DPPC bilayer with 128 lipids was prepared by cooling from 326 to 250 K at a rate of 0.253 K/ns. Note that the freezing/melting point of the SPC water model is 190 K.[45] This system was then replicated in one direction to get an elongated bilayer with 256 lipids, and the lipids were split into two regions whose boundary was perpendicular to that direction. The temperature of half of the lipids was set to 288 K so that this region remained in the gel phase. The other half was set at 353 K, so it melted into the fluid phase. The temperature of the water was set to 288 K. Pressure coupling was applied only in the direction perpendicular to the lipid phase boundaries. After melting half of the lipids, the temperature of the whole system was then changed to a temperature near the transition temperature. Lipids in the gel phase have dihedral angles in their tails close to the trans configuration (±60° around the trans configuration). The sign of the slope of the fraction of trans dihedrals in the lipid tails vs time indicates whether the current temperature is above or below the transition temperature. The magnitude of this slope is an indication of how far the current temperature is from the transition temperature. The coexistence method works well for pure DPPC, but it was not used for DPPC with lignin due to the difficulty in obtaining the correct distribution of lignin molecules throughout the system. The coexistence results did serve as a useful reference for comparison with the heating method discussed next.

Another way to estimate the transition temperature is to simply heat up the system until the transition is observed as in experiments. The problem with this approach is that the heating rates in MD simulations must necessarily be very high, which leads to overestimation of the transition temperature. As will be shown in the Results section, by comparing to the coexistence method, this overestimation was determined to be only a few degrees for pure DPPC systems. An advantage of this method is that it is simple and could be used for the systems containing DPPC and lignin molecules as easily as for pure DPPC systems.

The heating method was used with both a pure DPPC bilayer as well as systems with relatively high lignin dimer

DOI: 10.1021/acs.jpcb.9b05525
J. Phys. Chem. B 2019, 123, 8247−8260

concentrations of about 0.158 or 0.289 mole fraction of dimers relative to lipids. The relatively high concentrations were used to obtain significant shifts in the transition temperature. For bilayers with added lignin dimers, two different procedures were tried. In the first procedure, the fluid phase systems with lignin dimers were cooled from 326 to 250 K at a rate of 0.253 K/ns and held at 250 K for another 100 ns to create a gel phase. In the second procedure, lignin dimers were added to the solution outside the pure DPPC gel phase bilayer followed by equilibration before heating. All gel phase systems were heated back up from 250 to 326 K at the same rate as in cooling, so the systems transitioned back to the fluid phase. The transition temperature was determined only on the heating step, since it would be underestimated by a large amount in the cooling step due to the need to nucleate the ordered gel phase.

There are several quantities which might be used to determine the transition temperature. For a first order transition, there is a maximum in heat capacity at the transition temperature which also corresponds to a change in the slope of the enthalpy vs temperature. However, no observable change in the slope of the enthalpy could be found even for pure DPPC. This may indicate that the enthalpy change for the transition is small compared to the noise, or likely it is because the pure DPPC gel phase is defective or is a ripple phase. Despite trying various procedures, we could not obtain a defect free gel phase. This was also observed by Coppock and Kindt.[18] We tried using the bilayer thickness, the area per lipid, and the fraction of trans dihedrals in the lipid tails as used in the coexistence method. These quantities did show a slope change during the transition, but it was very small, leading to inaccuracy in determining the transition temperature. We found that the deuterium order parameters for the lipid tail atoms were a better measure and gave the clearest indication of the transition.

The deuterium order parameter, $S_{CD}(i)$, at various positions of ethylene groups along the hydrocarbon lipid tail is given by

$$S_{CD}(i) = \left\langle \frac{3\cos^2\theta - 1}{2} \right\rangle \tag{5}$$

where θ is the angle between the corresponding C−H bond vector and the bilayer normal. We used deuterium order parameters which were normalized and then averaged over carbon atoms 5−8 (see Figure 1 for carbon atom numbering) located in the middle of the lipid tails

$$S_{CD}^{norm} = \left\langle \frac{S_{CD}(i) - \overline{S_{CD}^{liq}(i)}}{\overline{S_{CD}^{gel}(i)} - \overline{S_{CD}^{liq}(i)}} \right\rangle_i \tag{6}$$

where $\overline{S_{CD}^{gel}(i)}$ and $\overline{S_{CD}^{liq}(i)}$ indicate time averages obtained in the gel and liquid phases and $\langle\ \rangle_i$ indicates an average over carbon atoms. S_{CD}^{norm} varies from around 1 in the gel phase to around 0 in the fluid phase and shows a change in slope during the transition. The transition temperature is taken as the temperature corresponding to the center of this transition region.

RESULTS

DSC Measurements of Transition Temperature. Differential scanning calorimetry (DSC) is a robust screening tool to study the lipid phase transitions as well as lipid−drug interactions, and is frequently used to identify the change in the thermodynamic lipid phase transition as a function of the concentration of components incorporated in the lipid bilayer.[46] Internalization of a solute in the lipid bilayer leads to a change in phase transition temperature (T_m) of the lipid bilayer.[47,48] The main phase transition temperature (T_m) of the lipid is a temperature at which the lipid membrane changes from a highly ordered 2D crystal-like gel state to a fluid-like state, and the pretransition temperature (T_p) is a temperature in which a flat membrane in the gel phase changes into a rippled bilayer.[49] The DSC instrument allows phase transition temperatures to be identified easily by a peak in the heat flow and, therefore, was applied to identify the gel−fluid transition temperature of liposomes in samples with and without lignin dimers.[28]

Figure 3 shows the DSC results measured for lignin dimer/liposome systems in PBS buffer (pH 7.4) on the second heating scan, after first heating from room temperature, cooling

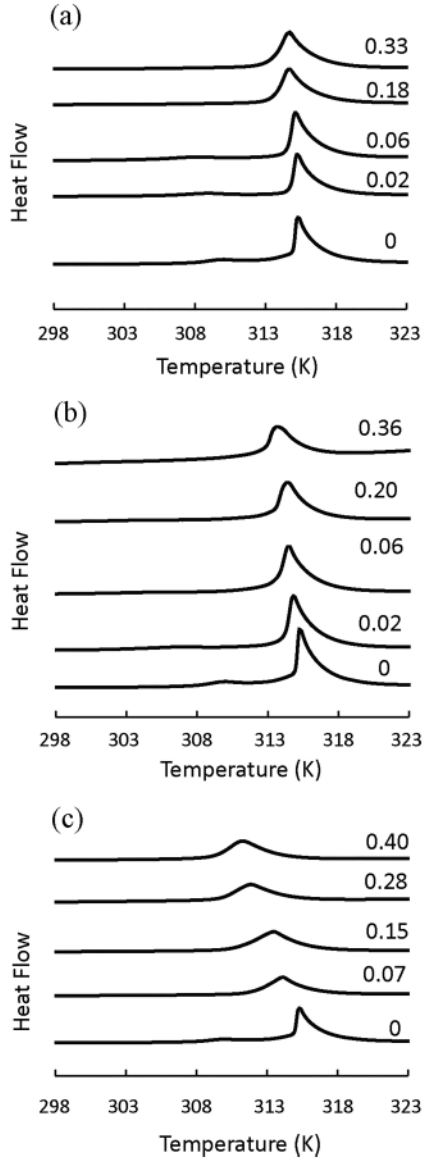

Figure 3. DSC heating scans for mixtures of DPPC with (a) G-βO4′-G, (b) G-βO4′-*trunc*G, and (c) *benz*G-βO4′-G. The mole fraction of the dimers is indicated beside each scan.

DOI: 10.1021/acs.jpcb.9b05525
J. Phys. Chem. B 2019, 123, 8247−8260

to 283 K, and heating again. The transition temperatures are consistent with the first heating scan (not shown), indicating that no significant artifacts of liposome preparation affected the results. The pure DPPC melting temperature (T_m) is indicated by a prominent endothermic peak at 315.5 ± 0.15 K, and the pure lipid also exhibits a pretransition at T_p = 310.8 K.[13] When a component incorporates into the lipid bilayer, a characteristic shift in the location of the endothermic peak related to the T_m happens, the magnitude of which depends on the concentration of the added component and strength of its interaction with the membrane.[47,48] The peaks in the heating thermograms for G-βO4′-G in Figure 3a show that, by increasing its mole fraction in the bilayer from X_{dimer} = 0 to X_{dimer} = 0.33, the main phase transition temperature is decreased from 315.5 to 314.7 K. In contrast, the results for DPPC/G-βO4′-*trunc*G (Figure 3b) show more significant shifts in T_m; as the dimer concentration increases from X_{dimer} = 0 to X_{dimer} = 0.36, T_m is decreased from 315.5 to 313.4 K. In the case of *benz*G-βO4′-G, the peaks in the heating thermographs (Figure 3c) also show a large effect on the gel-to-fluid phase transition; as the dimer concentration increases from X_{dimer} = 0 to X_{dimer} = 0.4, T_m is decreased from 315.5 to 311.5 K.

The melting temperatures of the DPPC/dimer samples for all three lignin GG dimers are included in Table 1. The results

Table 1. DSC Liquid Crystalline to Gel Transition Temperature in DPPC in the Presence of Lignin GG Dimers

G-βO4′-G		G-βO4′-*trunc*G		*benz*G-βO4′-G	
X_{dimer}	T_m (K)	X_{dimer}	T_m (K)	X_{dimer}	T_m (K)
0	315. 5	0	315.5	0	315.5
0.02	315.4	0.02	315.2	0.07	314.3
0.06	315.3	0.06	314.7	0.15	313.6
0.18	314.8	0.20	314.5	0.28	312.0
0.33	314.7	0.36	313.4	0.40	311.5

in this table clearly demonstrate that the presence of the G-βO4′-*trunc*G and *benz*G-βO4′-G dimers decreased T_m to a significant extent, while G-βO4′-G had only a slight effect. This suggests that G-βO4′-*trunc*G and *benz*G-βO4′-G partition into the interior hydrocarbon layer of the lipid bilayer to disrupt the order of the gel phase.

The partitioning of components into lipid bilayers and biological membranes is the foundation for drug uptake and passive transport into membranes and plays an important role in the molecular process of drug action.[50] Previously, the partition coefficients of some natural bioactive phenolic compounds in DPPC bilayers were measured.[51] Some of these plant-derived compounds which are known to have antimicrobial properties (such as eugenol, thymol, and carvacrol) have similar structures to lignin monomers.[52−54] Reiner et al. determined the partition coefficients of eugenol, thymol, carvacrol, propofol, and chlorothymol in DPPC membrane to be log(K) = 1.89, 2.64, 2.48, 3.06, and 3.54, respectively.[51] Here, the membrane partition coefficients of the lignin dimers are determined from eq 1 using linear regression of ΔT_m versus dimer concentration C_s in the limit of small C_s, as shown in Figure S1. Note that, at higher concentrations of the dimers, the depressions calculated from Table 1 deviate from a linear trend with C_s.[32] This is most likely caused by interactions among dimers that can cause clustering and significant perturbations of the gel phase. In contrast, there are negligible solute-based variations of the phases and solute−solute interactions in dilute solutions.[55] Therefore, we limited our measurements to the low concentrations of dimer where a linear relationship between ΔT_m and C_s was observed. As shown in this figure, ΔT increases linearly with increasing dimer concentration within the measured concentration range, and the slope increases with increasing hydrophobicity of the dimers. The results for the partition coefficients of all three lignin GG dimers are included in Table 2, and consistent with

Table 2. Comparison between log(K) from MD and Experiment

dimer	G-βO4′-G	G-βO4′-*trunc*G	*benz*G-βO4′-G
experiment (DSC)	2.72 ± 0.05	3.45 ± 0.20	3.38 ± 0.28
simulation (MD)	−1.42 ± 0.13	3.83 ± 0.29	5.21 ± 0.21

the slopes in Figure S1, log(K) is less for G-βO4′-G than for the G-βO4′-*trunc*G and for the *benz*G-βO4′-G dimers. This is consistent with the hydrophilic−lipophilic balance (HLB) of the dimers, which is calculated using the Davies group contribution method[56] to be 8.5 for G-βO4′-*trunc*G, 9.0 for G-βO4′-G, and 5.1 for *benz*G-βO4′-G. This corresponds to water dispersible character for the first two compounds but a high degree of lipophilicity for the latter.

The overall result of this calorimetry study supports the idea that partitioning into the lipid bilayer correlates with hydrophobicity/lipophilicity of the dimers.[57] The dimer most resembling natural lignin, G-βO4′-G, may associate with the bilayer, but its hydrophilic nature does not cause bilayer penetration. The commercially available truncated dimer, while it does contain a β-O-4 linker, is more hydrophobic and therefore has the ability to penetrate and disrupt the gel phase of DPPC bilayers. The benzyl derivative shows that it is possible to chemically alter naturally derived lignin compounds such that they are able to penetrate into lipid bilayers as well.

PMF Calculations for Dimers in Fluid Phase DPPC Bilayers. The MD calculations performed as part of this work allow us to gain greater insight not just into the general bilayer penetrating ability of dimers but also into where they prefer to reside and how their interactions alter the structure of the bilayers. The potential of mean force (PMF) curves as a function of the distance from the center of mass of single lignin dimers to the center of DPPC bilayers are shown in Figure 4.

The minimum in the G-βO4′-G curve is slightly outside the average position of the lipid phosphorus atoms, indicating that most of the natural lignin dimer resides at or near the exterior bilayer surface. There is a shoulder in the G-βO4′-G curve at distances between about 1.0 and 1.5 nm, indicating that there is a small probability of finding the dimer inside the bilayer. For the G-βO4′-*trunc*G curve, the minimum is inside the bilayer at around 1.2 nm. Therefore, most of the G-βO4′-*trunc*G resides inside the bilayer. There is a shoulder in the G-βO4′-*trunc*G curve at distances between about 1.9 and 2.3 nm, indicating that there is a small probability of finding the truncated dimers at the exterior bilayer surfaces. The minimum in the *benz*G-βO4′-G curve is around 1.0 nm which is even deeper in the bilayer than the minimum for G-βO4′-*trunc*G. The minimum is also more negative for *benz*G-βO4′-G than for G-βO4′-*trunc*G, about −20 k_BT compared to about −17 k_BT. There is also no shoulder in the *benz*G-βO4′-G at the bilayer surface, showing that it is expected to reside almost exclusively in the bilayer interior. These PMF results are

DOI: 10.1021/acs.jpcb.9b05525
J. Phys. Chem. B 2019, 123, 8247−8260

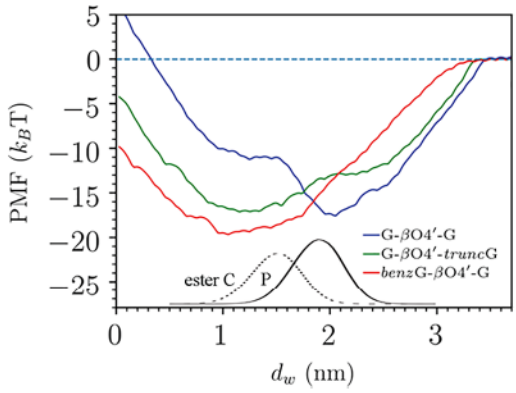

Figure 4. PMF curves for each of the three types of individual lignin dimers as a function of the distance from the dimer center of mass to the center of the lipid bilayer, d_w. The reference state is the dimer in bulk water, where the PMF is set to zero. For reference, the black solid and dashed lines trace the density distributions (scale not shown) for lipid phosphorus atoms (P) and lipid carbonyl carbon atoms in the ester groups (ester C).

qualitatively consistent with the experimental transition temperature shifts. Little of the natural G-βO4′-G dimer goes into the bilayer which leads to only small transition temperature shifts, while much more of the more hydrophobic G-βO4′-*trunc*G and *benz*G-βO4′-G dimers go into the bilayer, leading to larger transition temperature shifts. Even though PMFs provide insight into lignin dimer−DPPC interactions, they are possibly not that accurate due to incomplete convergence issues and systematic sampling errors. Larger solutes require more sampling or additional reaction coordinates to force more adequate sampling of conformations and orientations.[58]

Table 2 compares the log of the partition coefficients (log K) calculated using the PMF curves in Figure 4 with eq 4 using the average lipid phosphorus atom positions as the boundary between lipid and water phases with the experimental values estimated from T_m shifts. The simulation results show a similar trend compared to the experimental results in that the more hydrophobic G-βO4′-*trunc*G and *benz*G-βO4′-G have larger log K values than the more hydrophilic G-βO4′-G. However, the simulations predict larger differences in log K for the different dimers compared to experiment. Simulation results for log K range from −1.42 for *benz*G-βO4′-G to 5.21 for *benz*G-βO4′-G, while experimental results range from 2.72 to 3.45 for the same dimers. The negative value for G-βO4′-G just means that more of the molecules are found outside the phosphorus atom boundary than inside. Since most of G-βO4′-G is on the bilayer surface, choosing the boundary between phases somewhat outside the phosphorus atoms of the lipids would change the calculated log K significantly. Since this approach to comparison with experiment is only qualitative, we did not try to determine a way to define the boundary between phases more accurately. The MD simulations also predict that *benz*G-βO4′-G partitions more strongly into the bilayer than G-βO4′-*trunc*G, while experimental log K values of the two dimers are about the same.

Effect of Lignin Dimers on Fluid Phase Bilayer Structure. Prior to performing transition temperature calculations with MD simulations, we looked at the effect of the high concentrations of dimers on the structure of the bilayer in the fluid phase at 326 K. Increasing area per lipid is correlated with decreasing transition temperature. If lipids are more widely spaced in a fluid bilayer and therefore their tails are more disordered, then it requires a lower temperature to get them to transition to a gel phase with more ordered tails.

The FATSLIM program[59] was employed to perform an area per lipid (APL) calculation. FATSLIM gives an area for each lipid, so a distribution can be obtained and not just a mean value. The areas are obtained from a Voronoi tessellation of the projection of the lipid positions onto a plane which is perpendicular to the bilayer normal. The lipid position was defined by its headgroup, and the cutoff distance for neighbor searching was 3.0 nm.

Figure 5 shows the APL probability density (Pd) distributions for DPPC and for DPPC with various

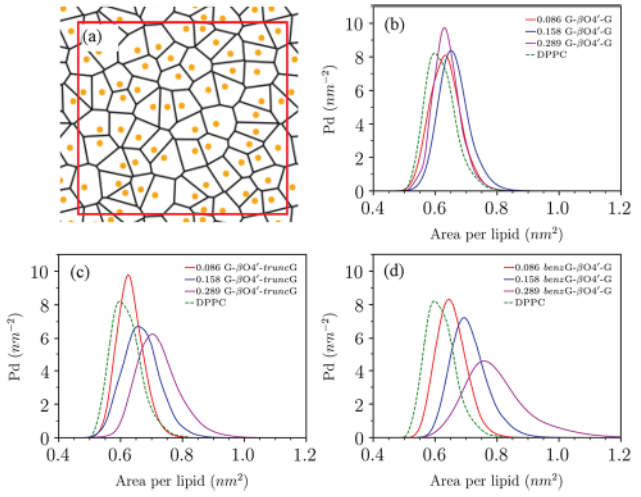

Figure 5. (a) Voronoi tessellation depicting the area distribution per lipid; orange dots indicate the position of the center of mass of lipid heads. Area per lipid probability density distributions (Pd) for DPPC bilayers and DPPC bilayers with added lignin dimers: (b) G-βO4′-G dimers, (c) G-βO4′-*trunc*G dimers, (d) *benz*G-βO4′-G dimers. The numbers in the legends indicate the mole fraction of lignin dimer relative to DPPC lipids.

concentrations of lignin dimers. The distributions for DPPC with G-βO4′-G in Figure 5b are all similar to the distribution for pure DPPC, regardless of the concentration. This is consistent with experimental results showing that G-βO4′-G does not shift the gel−fluid transition temperature much, even at high concentrations. The distributions for DPPC with G-βO4′-*trunc*G or *benz*G-βO4′-G in Figure 5c and d show clear increases in both the median APL and variance of the APL with increasing concentration. Consistent with the log(K) results from simulations, *benz*G-βO4′-G has the largest effect on APL at a given concentration due to its deep penetration into the lipid bilayers.

Phase Transition Temperatures from Molecular Dynamics. *Coexistence Method.* The coexistence method was used for pure DPPC as a reference for comparison to the heating method. After creating a system consisting of strips of gel and fluid phase bilayer, we first guessed a transition temperature of 308 K and performed a 200 ns NPT simulation at that temperature. We saw a noticeable growth in the fraction of gel phase at 308 K, so this temperature is lower than the transition temperature. We then simulated at a series of temperatures—312, 320, 316, 314, and 313 K—which allowed us to narrow down the transition temperature of pure DPPC to

DOI: 10.1021/acs.jpcb.9b05525
J. Phys. Chem. B 2019, 123, 8247−8260

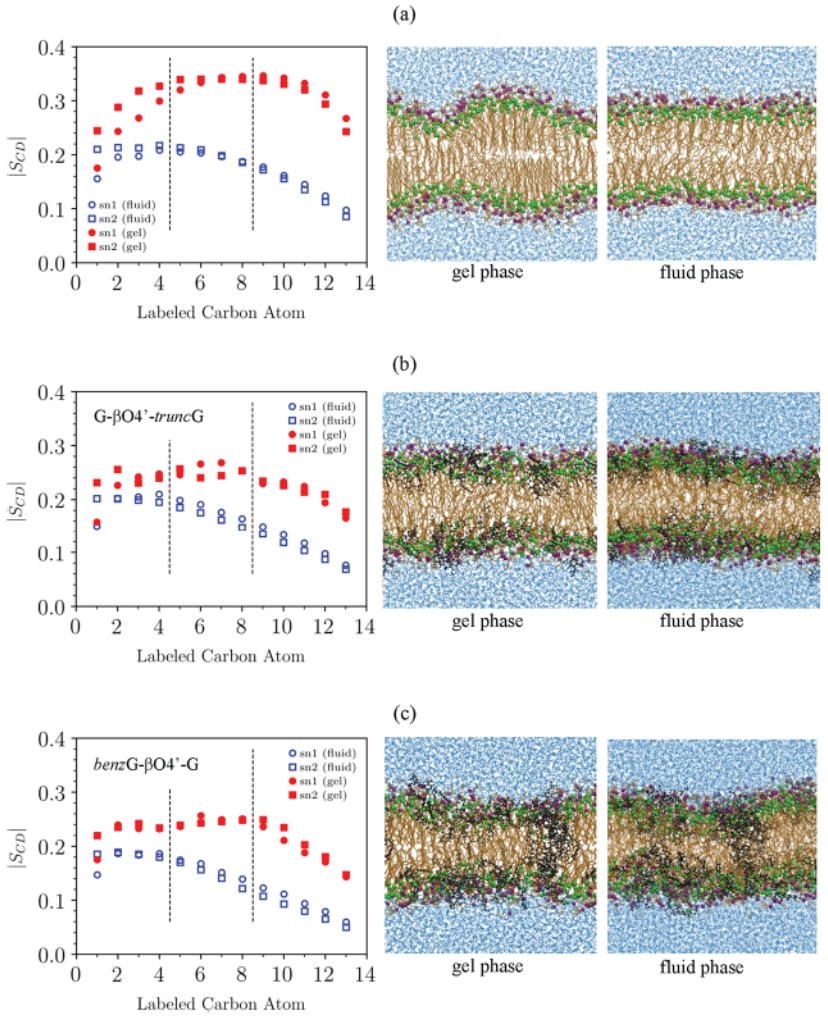

Figure 6. Deuterium order parameter, $|S_{CD}|$, for lipid tail sn1 and sn2 chains as a function of carbon atom index in liquid (326 K) and gel phase (250 K). Lower index atoms are closer to the lipid heads. The vertical dashed lines indicate the range of atoms which were used to obtain a normalized and averaged order parameter used to follow the phase transition. (a) 128 DPPC lipids. (b) 512 DPPC lipids with G-βO4′-*trunc*G dimers of concentration X_{dimer} = 0.289. (c) 512 DPPC lipids with *benz*G-βO4′-G dimers of concentration X_{dimer} = 0.289. Figures to the right of each plot were obtained from snapshots of the gel phase and liquid phase. In those pictures, lipids are represented in orange except for the ester carbon atoms (green) and phosphorus atoms (purple), lignin molecules are black, and water is blue (not all shown).

between 312 and 313 K which is quite close to the experimental main transition of 315.5 K found here, or of 314 K reported by Biltonen and Lichtenberg.[60]

Heating Method. The heating method was used for both pure DPPC and for DPPC with lignin dimers. These simulations were not performed for G-βO4′-G due to the small transition temperature shifts seen in experiments, the fact that it is found on the surface of the bilayer in simulations, and the small effect it has on area per lipid in simulations (Figure 5). Transition temperatures were obtained for bilayers containing G-βO4′-*trunc*G and *benz*G-βO4′-G.

Deuterium Order Parameter. Since the normalized deuterium order parameter averaged over several carbon atoms in the lipid tails is used as the indicator of the phase transition, we first show the deuterium order parameters for each system in both the fluid and gel phases in Figure 6. As expected, the difference between the fluid and gel phases for pure DPPC is larger than that for the systems with added lignin dimers. The biggest effect is in the gel phase; the lignin dimers do not allow the bilayer tails to become as ordered as in pure DPPC.

Metastable Gel Phase Bilayers Containing Lignin Dimers. Due to the high cooling rate, the gel phase structures containing lignin dimers may be in metastable states where lignin is trapped in the bilayer, while in the stable state the lignin may be largely expelled. Adding lignin to the outside of a pure DPPC gel phase followed by equilibration shows that the lignin dimers stay primarily on the surface of the gel phase bilayer. Although inaccurate at the low temperature of 250 K, PMF calculations also indicate that there should be a very small concentration of dimers inside the bilayer. Therefore, for calculation of transition temperature, we considered starting with the lignin trapped in the gel phase or with the lignin on the surface of the bilayer, since the latter is likely a better approximation. Note that we are still ignoring the partitioning of lignin dimers to the water phase. Considering this would be expensive, since instead of heating it would require doing several simulations at constant temperature with different dimer concentrations and those dimer concentrations would have to be first determined by PMF calculations which are difficult to obtain accurately, especially in the gel phase. We believe that starting with the lignin dimers outside the bilayer

DOI: 10.1021/acs.jpcb.9b05525
J. Phys. Chem. B 2019, 123, 8247−8260

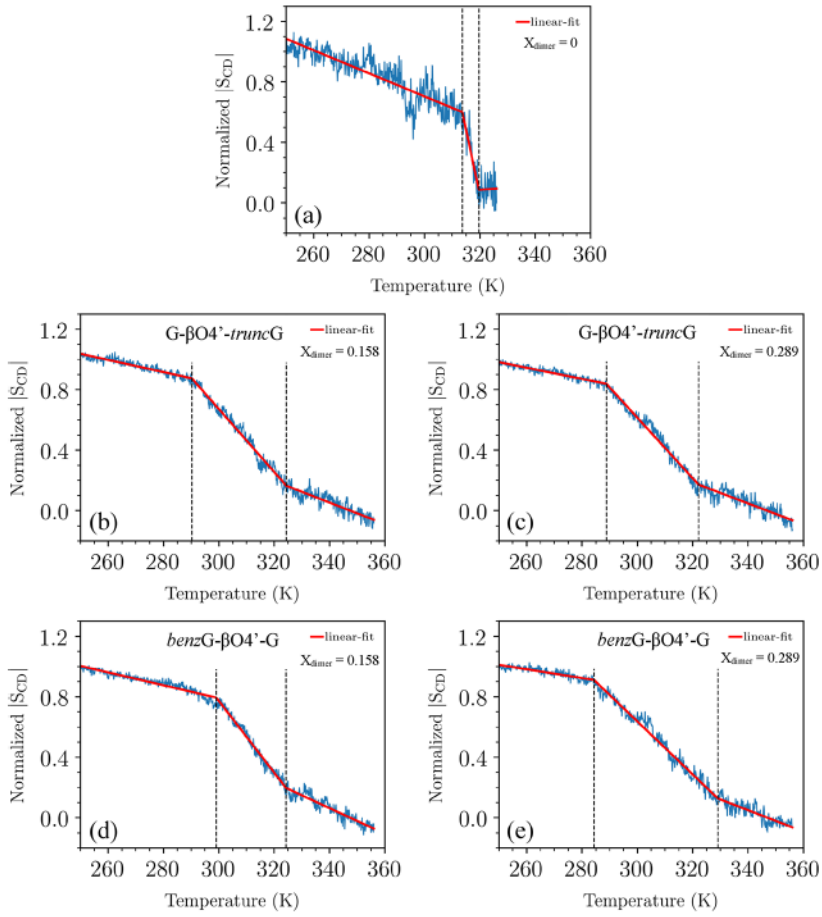

Figure 7. Normalized deuterium order parameter, $|S_{CD}|$, versus temperature and three-piece linear fits. (a) 128 DPPC lipids. (b and c) 512 DPPC lipids with G-βO4′-*trunc*G dimers of concentration X_{dimer} = 0.158 and 0.289, respectively. (d and e) 512 lipids with *benz*G-βO4′-G dimers of concentration X_{dimer} = 0.158 and 0.289, respectively. The vertical dashed lines indicate the turning points; the transition occurs between these lines, and the transition temperature is determined to be midway between them. The results in parts b−e are for the 512 DPPC lipid systems in which the lignin dimers were added to the solution outside of pure DPPC bilayers in the gel phase.

Table 3. Transition Temperatures (T_m) and Transition Widths (ΔT_{trans}) from MD Simulations[a]

N_{DPPC}	256[b]	128	512			
X_{dimer}	0	0	0.158		0.289	
dimer type	none	none	G-βO4′-*trunc*G	*benz*G-βO4′-G	G-βO4′-*trunc*G	*benz*G-βO4′-G
Simulations Starting with Dimers inside the DPPC Gel Phase						
T_m (K)	312.5[b]	316.6 ± 0.4	309.8 ± 1.8	309.3 ± 1.0	291.5 ± 1.6	292.2 ± 2.0
ΔT_{trans} (K)		6.0	30.0	35.1	38.6	52.3
Simulations Starting with Dimers outside the DPPC Gel Phase						
T_m (K)	312.5[b]	316.6 ± 0.4	307.3 ± 0.4	311.6 ± 0.4	305.4 ± 0.4	306.7 ± 0.6
ΔT_{trans} (K)		6.0	34.2	25.3	33.2	44.8

[a]N_{DPPC} is the number of DPPC lipid molecules. Transition widths are determined by the temperature difference between turning points shown in Figure 7. The transition temperature is defined to be midway between the turning points T_0 and T_1 shown in Figure 7; $T_m = (T_1 - T_0)/2$. Uncertainties were calculated by using 2 times the standard deviation from the mean value. (The details on the error estimation procedure are given in the Supporting Information.) [b]Coexistence method.

is a reasonable approximation, since they do not affect the bilayer structure much when on the surface (see plots of deuterium order parameters in the Supporting Information) and will naturally partition into the bilayer interior as the temperature is increased.

Transition Temperature. As seen in the snapshot in Figure 6a, a pure DPPC lipid bilayer does not form a perfect gel phase even at 250 K. A defective DPPC gel phase was also observed in Leekumjorn's study.[15] Despite this defect, the normalized S_{CD} shows a sharp drop in Figure 7a and the center of this drop gives a transition temperature of 316.6 K. This is higher than the results from the coexistence method of 312.5 K but only by about four degrees which is acceptable given the high heating rate.

With added lignin dimers, it is hard to visually determine from the snapshots in Figure 6 if the gel phase is formed but there is a clear increase in S_{CD} compared to the fluid phase seen in Figure 7b and c. The less ordered gel phase leads to a lower transition temperature, the transition occurs over a wider range of temperatures, and these effects are increased with

DOI: 10.1021/acs.jpcb.9b05525
J. Phys. Chem. B 2019, 123, 8247−8260

increasing lignin dimer concentration. This can be seen in the normalized S_{CD} plots as a function of temperature Figure 7b–e. For bilayers containing lignin dimers, both 128 and 512 lipid systems were considered. In some cases, determining the transition region was very difficult or impossible with only 128 lipids. Increasing the number of lipids also reduced the widths of the transition regions by about 10 K. Figure 7b–e shows only the results for the 512 lipid bilayer systems in which the lignin dimers were added to the solution outside the pure DPPC bilayers in the gel phase. The results for the 128 and 512 lipid systems with lignin added to DPPC bilayers while in the fluid phase are presented in the Supporting Information.

Table 3 summarizes the transition temperatures and transition widths from MD simulations. The lignin dimers G-βO4′-*trunc*G and *benz*G-βO4′-G had about the same effect on the transition temperature. The shifts relative to pure DPPC for X_{dimer} = 0.158 of G-βO4′-*trunc*G and *benz*G-βO4′-G are about 9 and 5 K, respectively, when the lignin dimers are started outside the gel phase bilayer. This is nearly the same compared to the case of starting with the dimers inside the bilayer where the shifts are both about 7 K. For low concentrations, trapping the lignin in the gel phase has little effect on the transition temperature. For X_{dimer} = 0.289 for G-βO4′-*trunc*G and *benz*G-βO4′-G, T_m shifts are about 11 and 10 K, respectively, when the lignin dimers are started outside the gel phase. This is significantly smaller than the case where the dimers start inside the bilayer where the shifts are about 24 and 23 K, respectively. This shows that, at high concentrations, the starting structure can be very important. Trapping the dimers in the bilayer leads to a much lower transition temperature, since the lignin molecules create disorder in the bilayer and lead to earlier onset of melting. The range of melting, ΔT_{trans}, is 5 and 8 K narrower for DPPC with X_{dimer} = 0.289 for G-βO4′-*trunc*G and *benz*G-βO4′-G, respectively, when the lignin dimers are started outside the gel phase. The MD results cannot be compared directly to experimental results, since experimental concentrations include all lignin in the system, while all lignin in MD systems is in the bilayer due to the small amount of water. The MD shifts for X_{dimer} = 0.158 are reasonable but likely large compared with experiment. The MD shifts for X_{dimer} = 0.289 are comparable when dimers are started outside of the bilayer but clearly too large from the opposite way. The MD results are qualitatively in line with experiments in that the effects of G-βO4′-*trunc*G and *benz*G-βO4′-G are similar, and the magnitude of the shifts increases with increasing concentration. Atomistic MD simulations of lipid phase transitions are difficult due to both time and length scale limitations. It may be possible to improve results by starting with more accurate concentrations determined from expensive PMF calculations in a series of constant temperature simulations as described above. Even with an extremely accurate calculation, it is still likely that the simulation parameters result in at least slightly different phase behavior than the real system. Although only qualitative in this case, the MD simulations still provide information about behavior at the molecular level that can be difficult to obtain from experiments.

The lack of a difference in transition temperatures between bilayers with G-βO4′-*trunc*G and *benz*G-βO4′-G in the MD simulations is surprising given that *benz*G-βO4′-G is larger and partitions more into the bilayer interior. However, this is consistent with experimental observations of similar log K values from DSC for the two dimers. This behavior might be explained by the fact that *benz*G-βO4′-G clustered together more than G-βO4′-*trunc*G inside the bilayer which can be seen visually in Figure 6b and c. Using all atoms in the molecules and a distance cutoff between atoms of 0.35 nm, the average cluster sizes for G-βO4′-*trunc*G and *benz*G-βO4′-G were 6 and 25, respectively. More clustering meant that there was more local disruption to the bilayer but perhaps less overall disruption. Even though there was less G-βO4′-*trunc*G in the bilayer interior, it spread out more, which caused more disruption and led to similar transition temperature shifts compared to *benz*G-βO4′-G.

■ CONCLUSIONS

Interactions between DPPC lipid bilayers and coniferyl alcohol-based lignin G–G dimers and their derivatives were studied using DSC experiments and MD simulations. Specifically, the systems studied consist of fully hydrated DPPC lipid bilayers and liposomes in the presence of different concentrations of lignin dimers for MD or DSC, respectively. Experimental liposome–water partition coefficients for the lignin dimers were obtained through a relationship between the shift in the gel–fluid transition temperature relative to pure DPPC liposomes obtained from DSC measurement. In MD simulations, partition coefficients were obtained using PMF calculations with a single dimer and a 128-DPPC bilayer. Transition temperatures in MD were estimated by first cooling the system to induce transition to the gel phase followed by heating to change back to the fluid phase. During the heating, we captured the transition from gel to fluid phase by defining and analyzing a normalized deuterium order parameter averaged over all carbon atoms located in the middle of the lipid tails. We further analyze the MD trajectories and study the location of the lignols and their effects on bilayer structure to explain the observed trends.

A commercially available truncated G–G dimer with the hydroxyproenyl tail removed, G-βO4′-*trunc*G, and G–G dimers with an added benzyl group, *benz*G-βO4′-G, show a higher affinity for the bilayer interior than natural dimers. DSC transition temperature shifts for the G-βO4′-G natural dimer were very small and consistent with that result. MD simulations showed that most of this dimer stays on the surface of the bilayer and has little effect on the lipid tail structure or area per lipid. The partition coefficient for the natural dimer was smallest from both DSC (2.72) and MD (log K = −1.42). The partition coefficients obtained using DSC measurements were similar for G-β4′-*trunc*G (log K = 3.45) and *benz*G-βO4′-G (log K = 3.38), while MD showed a higher partition coefficient for *benz*G-βO4′-G (log K = 5.21 compared to log K = 3.83) which is the most hydrophobic dimer considered.

Both G-βO4′-*trunc*G and *benz*G-βO4′-G dimers induced larger shifts in the gel–fluid phase transition in DSC compared to the natural dimer, and MD simulations for the transition temperature with natural dimer were not attempted due to the small shifts seen in DSC. The MD results show a very clear change in the deuterium order parameter associated with the transition for a pure DPPC bilayer with T_m = 316.5 K which is very close to the experimental value of 315.5 K. However, once hydrophobic lignin dimer derivatives are added to the system, the signal becomes noisier and wider, consistent with disorder caused by the lignin dimers and a coexistence region in the phase diagram, respectively. It is important to note that, with experimental systems, only the total amount of dimer added to

DOI: 10.1021/acs.jpcb.9b05525
J. Phys. Chem. B 2019, 123, 8247–8260

the experimental system is known, so that the amount that partitions into the bilayer will be less than the nominal amount added. In MD, all dimer was taken up by the bilayers; therefore, the transition temperature can give just a qualitative estimate. In the MD simulations, two types of starting configurations for the heating step were considered. In the first approach, the fluid phase with lignin was cooled down to obtain a gel phase. The potential problem with this is that it may trap the lignin inside the bilayer, leading to a metastable state. To alleviate this potential problem, the second type of configuration is obtained by adding lignin dimers outside a pure DPPC gel phase followed by equilibration before heating. This second type of starting configuration leads to significantly lower transition temperature shifts which are much closer to DSC results for high lignin concentrations but gives little difference compared to the first type of starting configuration at lower concentrations. MD transition temperature shifts were similar for G-βO4′-*trunc*G and *benz*G-βO4′-G, while DSC results predict slightly larger shifts for *benz*G-βO4′-G at high concentrations. The lack of difference in transition temperature shifts in MD simulations is surprising given that the MD calculated partition coefficient for *benz*G-βO4′-G was significantly larger. This may be due to increased clustering of *benz*G-βO4′-G in the bilayer relative to G-βO4′-*trunc*G leading to a reduced impact of *benz*G-βO4′-G on the overall bilayer structure.

Overall, this study shows that chemical modification of lignin dimers can have significant impacts on their interaction with model lipid bilayers. The comparison with experiments shows that these effects can be qualitatively captured using molecular dynamics simulations of lignin dimers at equilibrium and during heating of model lipid bilayers. MD simulations also provide details about the behavior of the molecules which is difficult to obtain from experiment. These results pave the way for using MD to screen other lignin oligomers and their derivatives with respect to their interactions with lipid bilayers.

■ ASSOCIATED CONTENT

Supporting Information

The Supporting Information is available free of charge on the ACS Publications website at DOI: 10.1021/acs.jpcb.9b05525.

> Linear fits to transition temperatures from DSC thermograms to obtain partition coefficient estimates; MD force field validation; transition temperature values when lignin dimers were added outside and equilibrated with the lipid bilayer in the fluid phase; the procedure for determination of turning points in the variation of the averaged normalized deuterium order parameter with temperature (PDF)

■ AUTHOR INFORMATION

Corresponding Author

*Phone: 225-578-6488. Fax: 225-578-5924. E-mail: dmoldo1@lsu.edu.

ORCID

Barbara L. Knutson: 0000-0001-5606-6226
Bert C. Lynn: 0000-0001-8426-3024
Dorel Moldovan: 0000-0001-7850-4207

Notes

The authors declare no competing financial interest.

■ ACKNOWLEDGMENTS

The authors gratefully acknowledge the support from the U.S. National Science Foundation under EPSCoR RII Track-2 Program (Project OIA-1632854). The computer resources were provided by Louisiana Optical Network Infrastructure (LONI) and High Performance Computing (HPC) at LSU.

■ REFERENCES

(1) Boija, E.; Johansson, G. Interactions between model membranes and lignin-related compounds studied by immobilized liposome chromatography. *Biochim. Biophys. Acta, Biomembr.* **2006**, *1758*, 620−626.

(2) Vinardell, M. P.; Mitjans, M. Lignins and their derivatives with beneficial effects on human health. *Int. J. Mol. Sci.* **2017**, *18*, 1219.

(3) Sato, S.; Mukai, Y.; Tokuoka, Y.; Mikame, K.; Funaoka, M.; Fujita, S. Effect of lignin-derived lignophenols on hepatic lipid metabolism in rats fed a high-fat diet. *Environ. Toxicol. Pharmacol.* **2012**, *34*, 228−234.

(4) Witzler, M.; Alzagameem, A.; Bergs, M.; Khaldi-Hansen, B. E.; Klein, S. E.; Hielscher, D.; Kamm, B.; Kreyenschmidt, J.; Tobiasch, E.; Schulze, M. Lignin-derived biomaterials for drug release and tissue engineering. *Molecules* **2018**, *23*, 1885.

(5) Figueiredo, P.; Lintinen, K.; Kiriazis, A.; Hynninen, V.; Liu, Z.; Bauleth-Ramos, T.; Rahikkala, A.; Correia, A.; Kohout, T.; Sarmento, B. In vitro evaluation of biodegradable lignin-based nanoparticles for drug delivery and enhanced antiproliferation effect in cancer cells. *Biomaterials* **2017**, *121*, 97−108.

(6) Baurhoo, B.; Ruiz-Feria, C.; Zhao, X. Purified lignin: Nutritional and health impacts on farm animals—A review. *Anim. Feed Sci. Technol.* **2008**, *144*, 175−184.

(7) Pan, X.; Kadla, J. F.; Ehara, K.; Gilkes, N.; Saddler, J. N. Organosolv ethanol lignin from hybrid poplar as a radical scavenger: relationship between lignin structure, extraction conditions, and antioxidant activity. *J. Agric. Food Chem.* **2006**, *54*, 5806−5813.

(8) Azadfar, M.; Gao, A. H.; Bule, M. V.; Chen, S. Structural characterization of lignin: A potential source of antioxidants guaiacol and 4-vinylguaiacol. *Int. J. Biol. Macromol.* **2015**, *75*, 58−66.

(9) Xü, Y.; Gietzen, K.; Galla, H.; Sackmann, E. Protein-mediated lipid transfer. The effects of lipid-phase transition and of charged lipids. *Biochem. J.* **1983**, *213*, 21−24.

(10) Jain, M. K.; Wu, N. M. Effect of small molecules on the dipalmitoyl lecithin liposomal bilayer: III. Phase transition in lipid bilayer. *J. Membr. Biol.* **1977**, *34*, 157−201.

(11) Saija, A.; Scalese, M.; Lanza, M.; Marzullo, D.; Bonina, F.; Castelli, F. Flavonoids as antioxidant agents: importance of their interaction with biomembranes. *Free Radical Biol. Med.* **1995**, *19*, 481−486.

(12) Hendrich, A. B.; Malon, R.; Pola, A.; Shirataki, Y.; Motohashi, N.; Michalak, K. Differential interaction of Sophora isoflavonoids with lipid bilayers. *Eur. J. Pharm. Sci.* **2002**, *16*, 201−208.

(13) Ojogun, V.; Vyas, S. M.; Lehmler, H. J.; Knutson, B. L. Partitioning of homologous nicotinic acid ester prodrugs (nicotinates) into dipalmitoylphosphatidylcholine (DPPC) membrane bilayers. *Colloids Surf., B* **2010**, *78*, 75−84.

(14) Zhao, L.; Feng, S.-S.; Kocherginsky, N.; Kostetski, I. DSC and EPR investigations on effects of cholesterol component on molecular interactions between paclitaxel and phospholipid within lipid bilayer membrane. *Int. J. Pharm.* **2007**, *338*, 258−266.

(15) Leekumjorn, S.; Sum, A. K. Molecular studies of the gel to liquid-crystalline phase transition for fully hydrated DPPC and DPPE bilayers. *Biochim. Biophys. Acta, Biomembr.* **2007**, *1768*, 354−365.

(16) Kowalik, B.; Schubert, T.; Wada, H.; Tanaka, M.; Netz, R. R.; Schneck, E. Combination of MD simulations with two-state kinetic rate modeling elucidates the chain melting transition of phospholipid bilayers for different hydration levels. *J. Phys. Chem. B* **2015**, *119*, 14157−14167.

DOI: 10.1021/acs.jpcb.9b05525
J. Phys. Chem. B 2019, 123, 8247−8260

(17) Qin, S. S.; Yu, Z. W.; Yu, Y. X. Structural characterization on the gel to liquid-crystal phase transition of fully hydrated DSPC and DSPE bilayers. *J. Phys. Chem. B* **2009**, *113*, 8114−8123.
(18) Coppock, P. S.; Kindt, J. T. Determination of phase transition temperatures for atomistic models of lipids from temperature-dependent stripe domain growth kinetics. *J. Phys. Chem. B* **2010**, *114*, 11468−11473.
(19) Waheed, Q.; Tjörnhammar, R.; Edholm, O. Phase transitions in coarse-grained lipid bilayers containing cholesterol by molecular dynamics simulations. *Biophys. J.* **2012**, *103*, 2125.
(20) Zhang, Y.; Lervik, A.; Seddon, J.; Bresme, F. A coarse-grained molecular dynamics investigation of the phase behavior of DPPC/cholesterol mixtures. *Chem. Phys. Lipids* **2015**, *185*, 88−98.
(21) Wang, Y.; Gkeka, P.; Fuchs, J. E.; Liedl, K. R.; Cournia, Z. DPPC-cholesterol phase diagram using coarse-grained molecular dynamics simulations. *Biochim. Biophys. Acta, Biomembr.* **2016**, *1858*, 2846−2857.
(22) Duncan, S. L.; Dalal, I. S.; Larson, R. G. Molecular dynamics simulation of phase transitions in model lung surfactant monolayers. *Biochim. Biophys. Acta, Biomembr.* **2011**, *1808*, 2450−2465.
(23) Liu, C.-J.; Miao, Y.-C.; Zhang, K.-W. Sequestration and transport of lignin monomeric precursors. *Molecules* **2011**, *16*, 710−727.
(24) Miao, Y.-C.; Liu, C.-J. ATP-binding cassette-like transporters are involved in the transport of lignin precursors across plasma and vacuolar membranes. *Proc. Natl. Acad. Sci. U. S. A.* **2010**, *107*, 22728−22733.
(25) Perkins, M.; Smith, R. A.; Samuels, L. The transport of monomers during lignification in plants: anything goes but how? *Curr. Opin. Biotechnol.* **2019**, *56*, 69−74.
(26) Sibout, R.; Höfte, H. Plant cell biology: the ABC of monolignol transport. *Curr. Biol.* **2012**, *22*, R533−R535.
(27) Besombes, S.; Mazeau, K. The cellulose/lignin assembly assessed by molecular modeling. Part 2: seeking for evidence of organization of lignin molecules at the interface with cellulose. *Plant Physiol. Biochem.* **2005**, *43*, 277−286.
(28) Demetzos, C. Differential Scanning Calorimetry (DSC): a tool to study the thermal behavior of lipid bilayers and liposomal stability. *J. Liposome Res.* **2008**, *18*, 159−73.
(29) Asare, S. O.; Kamali, P.; Huang, F.; Lynn, B. C. Application of chloride adduct ionization tandem mass spectrometry for characterizing and sequencing synthetic lignin model compounds. *Energy Fuels* **2018**, *32*, 5990−5998.
(30) Szoka, F., Jr; Papahadjopoulos, D. Comparative properties and methods of preparation of lipid vesicles (liposomes). *Annu. Rev. Biophys. Bioeng.* **1980**, *9*, 467−508.
(31) Olson, F.; Hunt, C.; Szoka, F.; Vail, W.; Papahadjopoulos, D. Preparation of liposomes of defined size distribution by extrusion through polycarbonate membranes. *Biochim. Biophys. Acta, Biomembr.* **1979**, *557*, 9−23.
(32) Inoue, T.; Miyakawa, K.; Shimozawa, R. Interaction of surfactants with vesicle membrane of dipalmitoylphosphatidylcholine. Effect on gel-to-liquid-crystalline phase transition of lipid bilayer. *Chem. Phys. Lipids* **1986**, *42*, 261−270.
(33) Lindahl, E.; Hess, B.; Van Der Spoel, D. GROMACS 3.0: a package for molecular simulation and trajectory analysis. *J. Mol. Model.* **2001**, *7*, 306−317.
(34) Bussi, G.; Donadio, D.; Parrinello, M. Canonical sampling through velocity rescaling. *J. Chem. Phys.* **2007**, *126*, 014101.
(35) Schmid, N.; Eichenberger, A. P.; Choutko, A.; Riniker, S.; Winger, M.; Mark, A. E.; van Gunsteren, W. F. Definition and testing of the GROMOS force-field versions 54A7 and 54B7. *Eur. Biophys. J.* **2011**, *40*, 843.
(36) Berendsen, H. J.; Postma, J. P.; van Gunsteren, W. F.; Hermans, J. Interaction models for water in relation to protein hydration. *Intermolecular forces*; Springer: 1981; pp 331−342.
(37) Malde, A. K.; Zuo, L.; Breeze, M.; Stroet, M.; Poger, D.; Nair, P. C.; Oostenbrink, C.; Mark, A. E. An automated force field topology builder (ATB) and repository: version 1.0. *J. Chem. Theory Comput.* **2011**, *7*, 4026−4037.
(38) Langer, V.; Lundquist, K.; Miksche, G. E. erythro-2-(2, 6-Dimethoxy-4-methylphenoxy)-1-(4-hydroxy-3, 5-dimethoxyphenyl) propane-1, 3-diol. *Acta Crystallogr., Sect. E: Struct. Rep. Online* **2005**, *61*, o1001−o1003.
(39) Domański, J.; Stansfeld, P. J.; Sansom, M. S.; Beckstein, O. Lipidbook: a public repository for force-field parameters used in membrane simulations. *J. Membr. Biol.* **2010**, *236*, 255−258.
(40) Martínez, L.; Andrade, R.; Birgin, E. G.; Martínez, J. M. PACKMOL: a package for building initial configurations for molecular dynamics simulations. *J. Comput. Chem.* **2009**, *30*, 2157−2164.
(41) Kästner, J. Umbrella sampling. *Wiley Interdiscip. Rev. Comput. Mol. Sci.* **2011**, *1*, 932−942.
(42) Souaille, M.; Roux, B. t. Extension to the weighted histogram analysis method: combining umbrella sampling with free energy calculations. *Comput. Phys. Commun.* **2001**, *135*, 40−57.
(43) Zocher, F.; van der Spoel, D.; Pohl, P.; Hub, J. S. Local partition coefficients govern solute permeability of cholesterol-containing membranes. *Biophys. J.* **2013**, *105*, 2760−2770.
(44) Jakobtorweihen, S.; Zuniga, A. C.; Ingram, T.; Gerlach, T.; Keil, F.; Smirnova, I. Predicting solute partitioning in lipid bilayers: Free energies and partition coefficients from molecular dynamics simulations and COSMOmic. *J. Chem. Phys.* **2014**, *141*, 045102.
(45) Vega, C.; Sanz, E.; Abascal, J. The melting temperature of the most common models of water. *J. Chem. Phys.* **2005**, *122*, 114507.
(46) McElhaney, R. N. The use of differential scanning calorimetry and differential thermal analysis in studies of model and biological membranes. *Chem. Phys. Lipids* **1982**, *30*, 229−59.
(47) Chiu, M. H.; Prenner, E. J. Differential scanning calorimetry: An invaluable tool for a detailed thermodynamic characterization of macromolecules and their interactions. *J. Pharm. BioAllied Sci.* **2011**, *3*, 39−59.
(48) Maeda, Y.; Nunomura, K.; Ohtsubo, E. Differential scanning calorimetric study of the effect of intercalators and other kinds of DNA-binding drugs on the stepwise melting of plasmid DNA. *J. Mol. Biol.* **1990**, *215*, 321−9.
(49) Riske, K. A.; Barroso, R. P.; Vequi-Suplicy, C. C.; Germano, R.; Henriques, V. B.; Lamy, M. T. Lipid bilayer pre-transition as the beginning of the melting process. *Biochim. Biophys. Acta, Biomembr.* **2009**, *1788*, 954−63.
(50) De Young, L. R.; Dill, K. A. Solute partitioning into lipid bilayer membranes. *Biochemistry* **1988**, *27*, 5281−5289.
(51) Reiner, G. N.; Labuckas, D. O.; García, D. A. Lipophilicity of some GABAergic phenols and related compounds determined by HPLC and partition coefficients in different systems. *J. Pharm. Biomed. Anal.* **2009**, *49*, 686−691.
(52) Marchese, A.; Orhan, I. E.; Daglia, M.; Barbieri, R.; Di Lorenzo, A.; Nabavi, S. F.; Gortzi, O.; Izadi, M.; Nabavi, S. M. Antibacterial and antifungal activities of thymol: A brief review of the literature. *Food Chem.* **2016**, *210*, 402−414.
(53) Marinelli, L.; Di Stefano, A.; Cacciatore, I. Carvacrol and its derivatives as antibacterial agents. *Phytochem. Rev.* **2018**, *17*, 903−921.
(54) Barber, M. S.; McConnell, V. S.; DeCaux, B. S. Antimicrobial intermediates of the general phenylpropanoid and lignin specific pathways. *Phytochemistry* **2000**, *54*, 53−56.
(55) Heerklotz, H. Interactions of surfactants with lipid membranes. *Q. Rev. Biophys.* **2008**, *41*, 205−264.
(56) Kuentz, M. T.; Arnold, Y. Influence of molecular properties on oral bioavailability of lipophilic drugs−mapping of bulkiness and different measures of polarity. *Pharm. Dev. Technol.* **2009**, *14*, 312−320.
(57) Koynova, R.; Caffrey, M. Phases and phase transitions of the phosphatidylcholines. *Biochim. Biophys. Acta, Rev. Biomembr.* **1998**, *1376*, 91−145.
(58) Neale, C.; Pomès, R. Sampling errors in free energy simulations of small molecules in lipid bilayers. *Biochim. Biophys. Acta, Biomembr.* **2016**, *1858*, 2539−2548.

DOI: 10.1021/acs.jpcb.9b05525
J. Phys. Chem. B 2019, 123, 8247−8260

(59) Buchoux, S. FATSLiM: a fast and robust software to analyze MD simulations of membranes. *Bioinformatics* **2017**, *33*, 133−134.
(60) Biltonen, R. L.; Lichtenberg, D. The use of differential scanning calorimetry as a tool to characterize liposome preparations. *Chem. Phys. Lipids* **1993**, *64*, 129−142.

DOI: 10.1021/acs.jpcb.9b05525
J. Phys. Chem. B 2019, 123, 8247−8260